Title

Modulating motility of intracellular vesicles in cortical neurons with nanomagnetic forces on-chip

Journal

Lab on a Chip, 17(5)

ISSN

1473-0197

Authors

Kunze, Anja
Murray, Coleman Tylor
Godzich, Chanya
et al.

Publication Date

2017-02-28

DOI

10.1039/c6lc01349j

Peer reviewed

Published in final edited form as:

Lab Chip. 2017 February 28; 17(5): 842–854. doi:10.1039/c6lc01349j.

Modulating motility of intracellular vesicles in cortical neurons with nanomagnetic forces on-chip

Anja Kunze[1,4,*], **Coleman Tylor Murray**[1], **Chanya Godzich**[1], **Jonathan Lin**[1], **Keegan Owsley**[1], **Andy Tay**[1], and **Dino Di Carlo**[1,2,3,*]

[1]Department of Bioengineering, University of California, Los Angeles, California 90095, United States

[2]California NanoSystems Institute, University of California, Los Angeles, California 90095, United States

[3]Jonsson Comprehensive Cancer Research Center, University of California, Los Angeles, California 90095, United States

[4]Department of Electrical and Computer Engineering, Montana State University, Bozeman, Montana 59717, United States

Abstract

Vesicle transport is a major underlying mechanism of cell communication. Inhibiting vesicle transport in brain cells results in blockage of neuronal signals, even in intact neuronal networks. Modulating intracellular vesicle transport can have a huge impact on the development of new neurotherapeutic concepts, but only if we can specifically interfere with intracellular transport patterns. Here, we propose to modulate motion of intracellular lipid vesicles in rat cortical neurons based on exogenously bioconjugated and cell internalized superparamagnetic iron oxide nanoparticles (SPIONs) within microengineered magnetic gradients on-chip. Upon application of 6–126 pN on intracellular vesicles in neuronal cells, we explored how the magnetic force stimulus impacts the motion pattern of vesicles at various intracellular locations without modulating the entire cell morphology. Altering vesicle dynamics was quantified using, mean square displacement, a caging diameter and the total traveled distance. We observed a de-acceleration of intercellular vesicle motility, while applying nanomagnetic forces to cultured neurons with SPIONs, which can be explained by a decrease in motility due to opposing magnetic force direction. Ultimately, using nanomagnetic forces inside neurons may permit us to stop the mis-sorting of intracellular organelles, proteins and cell signals, which have been associated with cellular dysfunction. Furthermore, nanomagnetic force applications will allow us to wirelessly guide axons and dendrites by exogenously using permanent magnetic field gradients.

*Corresponding authors: anja.kunze@montana.edu, dicarlo@seas.ucla.edu.

Author Contributions

A.K. designed, performed, analyzed chips and experiments, interpreted data, wrote and revised the manuscript. C.M. fabricated chips, wrote and revised the manuscript. C.G. assisted with experiments wrote and revised supplementary data. K.O. developed and performed numerical simulations, and wrote the manuscript. J.L. provided differentiated human neurons, wrote the manuscript. A.T. characterized nanoparticle uptake. D.D. interpreted data, wrote and revised the manuscript.

Competing Financial Interests

The authors of this manuscript declare no competing financial interest.

Graphical abstract

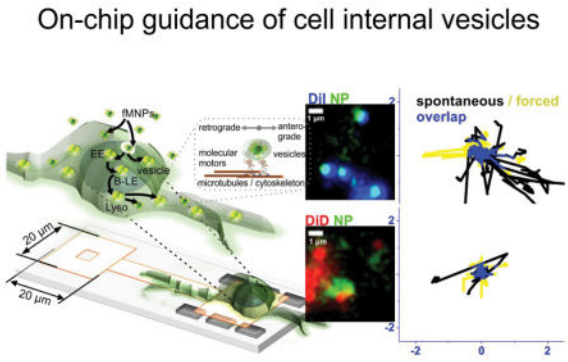

Introduction

The role of mechanical forces in neuronal cell behavior in the central nervous system has long been neglected in neuroscience, until recent links between mechanical perturbations and axon potential firing were found.[1, 2] Today we know that mechanical forces or tension are involved in the formation of the cortical landscape folding,[3] in neuronal cell morphology,[4, 5] in neurite or axonal outgrowth,[6–10] in synaptic functioning,[1, 11] and in signal transduction[12, 13] through mechanically activated ion channels.[14, 15] A majority of these results are derived from *in vitro* experiments, where the mechanical stimulus was externally positioned. Applying external forces through glass micropipettes,[5, 16, 17] magnetic/optical tweezers,[18–21] or stretchable cell platforms,[6, 11, 22] impart mechanical bending, compression, or expansion on the cell plasma membrane. Within this context it was reported that stretching axons resulted in faster accumulation of synaptic vesicles at the growth cone compared to un-stretched neurons.[13] But can intracellular mechanical stimulation influence vesicle transport? Answering this question will open ways to use nanoparticle-mediated biomechanical forces, which we call nanomagnetic forces, to interfere with neural pathways and their role and resolution in disease processes. To study a direct force impact on transport behavior of intracellular vesicles, we utilize chitosan-coated superparamagnetic nanoparticles (Chi-NP), which become internalized in neurons through cell intrinsic uptake mechanism such as endocytosis and phagocytosis.[23] Exposing Chi-NPs to engineered magnetic field gradients on chip allows us to modulate vesicle trafficking within sub-populations of lipid vesicles in the intracellular space.

Neurobiologists hypothesize that neurons translocate membrane compartments and proteins through vesicles.[24] The resulting traffic of vesicles in neurons consists of a wide variety of components and is a critical factor in the development of cell polarity and neurodegeneration. First, the transported cargos are either membranous vesicles (early-/late-endosomes, to multi-vesicular endosome, lysosomes, or lipid vesicles), mRNA transporters, synaptic precursor protein vesicles, receptor vesicles, or growth factor transporting vesicles.[25] Second, they bind to microtubules by kinesin and dynein motors and are transported along them in anterograde and retrograde directions (away from and towards the cell nucleus), by showing a diverse set of motion patterns, e.g. fast directed transport, locally

"caged" circuits, or almost immobilized "docked" behavior.[25, 26] The amount and type of vesicles, as well as their transport behavior, depend on the cell developmental and functional state.[1, 14] Third, during neuronal development a neuron exhibits an asymmetric cell morphology resulting in the formation of an axon and multiple dendrites. This cell polarization process involves the sorting of Tau and Map2 proteins in the specific axonal and dendritic cell compartment, to build up and stabilize the cytoskeleton there.[27, 28] Thus, during polarization a neuron has to differentially organize its vesicles into functionally opposite cell compartments.

Impaired vesicle transport can lead to mis-sorting of proteins resulting in developmental disorders or neurodegeneration.[29] Considering the example of the protein Tau during axonal development, the more developed the cytoskeleton, the more vesicles can interfere with Tau proteins potentially slowing down transport.[30] An overexpression of Tau in neuroblastoma cells has been shown to impair the transport of mitochondria in neurites.[31, 32] The same group proposed that Tau differentially regulates the attachment and detachment but not the speed of kinesin motors, [27] which leads to a Tau gradient with a low concentration in the soma and high concentration near the growth cone. [30, 33] Dixit *et al.* proposed that an inverted Tau concentration gradient with high concentrations of Tau near the soma might regulate degeneration processes in neurons. Thus, through engineering Tau concentrations in neurons we may prevent neurons from degenerating their networks, especially, when no other growth cues are available. In this context, we have shown previously that a nanomagnetic force stimulus 5 – 70 pN, applied over 24 hours, locally modulated Tau distribution in cortical neurons [34] While the translocation of Tau was related to the nanomagnetic force strength, how vesicle transport gets impacted under the application of nanomagnetic forces remains an open question.

Here we investigate how intracellular nanomagnetic forces can impact the transport pattern of lipophilic dye labeled vesicles in cortical neurons over short time scales (Fig. 1). Using previously developed arrays of magnetizable permalloy elements,[34, 35] we applied localized forces on nanoparticle-laden vesicles to explore the effect of force on the motility of vesicles in a highly-parallelized manner (Fig. 2a1 – a3).

Experimental

Neuronal cell culture and endosomal labeling

Rat cortical hemispheres were dissected from whole embryonic rat brains (E18, BrainBits) and dissociated with 10 % (v/v) Papain (Carica papaya, Roche) in Hibernate®-E (BrainBits) at 35 °C for 15 min. After dissociation, cortical neurons were centrifuged (6 min, 600 rpm, at room temperature) and seeded at a cell concentration of 2×10^6 cells/ml, drop wise on-chip (150 – 300 µl). Unbound cells were removed after 2 h incubation through a gentle washing step and incubated overnight (95 % air, 5 % CO_2, 37 °C) in Neurobasal serum free with 2 % (v/v) serum free B-27®, 1% (v/v) GlutaMAX™ and 1% (v/v) Pen Strep. Pre-differentiated, mixed population neurons derived from human induced pluripotent stem cells (human iPSC line, XCL-1) were thawed drop-wise in 37°C neuronal medium (Neuro Kit, XN-001-S-NH, Xcell Science) and counted on a hemocytometer following resuspension. Cells were then seeded at 2×10^6 cells/ml density by placing 250 µl on-chip and cultured in complete

neuronal medium for the remainder of the study. To visualize different intracellular vesicle types in rat cortical neurons we used CellLight® Late Endosomes-RFP, BacMam 2.0 to fluorescently label Rab7a proteins in late endosomes, and two lipophilic dyes: Vybrant® DiI (1,1′-dioctadecyl-3,3,3′,3′-tetramethyl-indodicarbocyanine 4-chlorobenzenesulfonate salt) and DiD (1,1′-dioctadecyl-3,3,3′,3′-tetra-methylindocarbocyanine perchlorate) Cell-Labeling Solution to highlight intracellular lipid vesicles and LysoTracker® Deep Red to stain acidic lysosomes. RFP late endosomal transfection was combined with DiD (Far-red fluorescent) vesicle staining or Deep Red LysoTracker staining and with DiI (red-fluorescent) with DiD or LysoTracker. Baculovirus transfection of Rab7a was started 16 h prior to nanoparticle exposure in neurons at day one in culture with 50 particles per cell. LysoTracker labeling was optimal when loaded 2 h prior to imaging at a final concentration of 100 nM in 5 ml. DiD and DiI staining was achieved following vendor protocol. Prior to nanoparticle incubation, 100 μl of a 0.5% (v/v) DiI or DiD/media solution was administered to neurons on-chip, incubated up to 1 h and subsequently gently washed with pre-warmed culture media (2x).

Highly parallelized on-chip nanomagnetic force induction

To impose an intracellular mechanical force, cortical neurons were incubated with 30 μg/ml chitosan or dextran bio-conjugated green fluorescent iron oxide nanoparticles (superparamagnetic, $h_{d,vendor}$ = 100 nm, nano-screenMAG/G-Chitosan or -D, Chemicell) for six hour prior to experimental manipulation. Unconjugated iron oxide nanoparticle were shown to induce cytotoxic effects in neuronal-like cells[36, 37] and were used for reference measurements only, see in Supplementary Information. Residual medium containing unabsorbed nanoparticles was removed and neurons were washed with pre-warmed media. Neuromagnetic chips were then transferred to the imaging platform and immersed into CO_2-independent pre-warmed Hibernate E Low Fluorescence imaging media (BrainBits). Prior to magnetic force induction vesicle motion was recorded and individual cell position saved for additional experimental procedures (no magnetic force experiment). A neodymium magnet B_{max} = 150 mT (½ inch × ½ inch × ½ inch, Apex Magnets) was placed on the top right side of the neuromagnetic chip to expose the culture to a permanent magnetic field and to allow phase contrast microscopy. Vesicle movement was monitored with a delay of 1 – 2 min after magnetic field and force induction (with magnetic force experiment).

Within magnetic field gradients a mechanical force imposes on the superparamagnetic nanoparticles. Local magnetic field gradients were generated through ferromagnetic iron nickel alloys called magnetic elements (MEs) on chip within a permanent magnetic field. The force range for different cluster sized fMNPs has been characterized previously[34] using Stoke's and Faxen's law and were re-confirmed here through COMSOL simulation. Briefly, 4 μm × 8 μm × 4 μm (H × L × T) MEs generated a magnetic field gradient of ~ 20 A/m^2 within a permanent magnetic field (B_{max} = 150 mT, d_z = 1.5 mm, ½ in. × ½ in. × ½ in., Apex Magnets). Correlation between magnetic element size and particle volume dependent magnetic forces was previously estimated[34]. Nanoparticle clusters of r = 400 nm, 490 nm and 750nm resulted in $F_{max,\ x=1\ \mu m}$ = 6.1 – 19.2 pN, 11.3 – 35.3 pN and 40.1 – 125.7 pN, respectively. The resulting magnetic force stimulation area on-chip consisted of an array of six MEs (2 × 3, 4 μm × 8 μm), 16 μm spaced in x-direction and 4 μm spaced in y-direction;

or of three MEs in one column 16 μm spaced. The cell adhesion pattern was in symmetry above the ME array covering a surface of 20 μm × 20 μm. A pattern line (7.5 μm wide and 50 μm – 100 μm long) connected the cell pattern region with MEs with an ME empty cell region. The resulting magnetic field strength and magnetic field gradient pattern near the magnetic elements are shown in figure S1 in Supplementary Information.

Biochemically blocking and activating liposomal motion

Biochemically altering vesicle transport was achieved through blocking and activating vesicle movement using monastrol[38–41] and insulin,[42] respectively. For blocking, we prepared 1 mM monastrol (Sigma, M8515) stock solution by dissolving lyophilized powder (≥98%, HPLC) in DMSO. An aliquot of 100 μl was dissolved in 1 ml Hibernate E and chips were immersed into imaging solution and let incubated for 10 min prior to imaging. Vesicle transport was accelerated through the addition of 10% (v/v) human insulin (Sigma, I9278, 10mg/ml stock), to media in the imaging platform, where neurons were incubated for at least 20 min prior imaging. Note: Insulin concentration was intentionally chosen high above physiological condition[43] to activate a cells response within few minutes.

Image acquisition and analysis

Life cell imaging of fluorescently labeled vesicles in cortical neurons were semi-automated captured using a programmable stage (MIV-2000 Te/Ti 2000 He, ASIimaging) on a Nikon microscope (Eclipse Ti, DAPI, FITC, TRICT, CY-5 filters, 60x air, NA = 0.85, and 60x oil, NA = 1.4 objectives) with a CCD camera (QuantEM:512SC EM, Photometrics) operated at fixed gain. Cell position was captured and referenced with magnets applied in positive-X-axis pointing towards right. Channel exposure times were set to CY-5: 800 ms, TRITC: 800 ms and FITC: 500 ms. Multi-channel image acquisition was programmed with 3 s – 6 s time intervals to capture 3 channels/time point. Multi-channel time stacks, which contained vesicle position $x_{n,p}(t_p)$ $y_{n,p}(t_p)$ with n number of vesicles and p position at multiple time points t_p, were further processed as 8-bit color image sequence, corrected for transformative shift with StackReg[44] plugin (ImageJ) in case of occurrence and histogram corrected for auto bleaching. Subsequent, moving vesicle dots were tracked using TrackMate[45] (DOG detector,[46] 0.8 μm blob diameter; filters: median intensity, estimated diameter and signal/noise ratio; linking: 1.6 μm) and exported into .xml files. A MATLAB script excludes tracks shorter than 108 s, generated star plots for tracks (Δt_{max} = 2 min), computes mean square displacement[47] (MSD, Δt = 57 s, $\boldsymbol{\tau}$ = 3 *s*, $MSD=\frac{1}{p-\tau}\sum_{\tau=1}^{p-\tau}\left|\begin{pmatrix} x_{i+1} \\ y_{i+1} \end{pmatrix}-\begin{pmatrix} x_i \\ y_i \end{pmatrix}\right|^2$), averaged "caging" diameter[48] (CD, Δt = 114 s, $CD_{avg}=\frac{1}{k}\sum_{i=1}^{k=\frac{t_{max}}{\tau}} CD_i(t_i)$), total traveled length (L, Δt = 114 s, $L_{total}=\sum_{i=1}^{p} L_i$) and averaged velocity (all n tracks, $V_{avg}=\frac{1}{p}\sum_{i=1}^{p}\frac{L_i}{t_i-t_{i-1}}$) and outputs frequency for categorized vesicle behavior based on CD and L. MSD of vesicle tacks were then compared with MSD model[47] (2D case) of stationary processes for free diffusion ($MSD_{diff} = 4D\boldsymbol{\tau}$), intracellular free diffusion ($MSD_{cell} = 4\ k_{cell}\ D_{H_2O}\boldsymbol{\tau}$) and confined diffusion ($MSD_{conf}=R_c^2(1-e^{-4k_{cell}D_{H_2O}\tau/R_c^2})$, with k_{cell} = 0.05, *Stokes − Einstein:* D_{H_2O} at 37°).

Statistical analysis

Velocity and length distributions were tested against Normality distribution appropriate ANOVAs were chosen based on parametric and non-parametric test routines (OriginPro 9, $p<0.001$ or otherwise indicated). Histogram distribution of CD-L categories were compared using Chi-Square test[49] and were visualized based on $p > 0.05$ (not significant) and $p \leq 0.05$ (significant different).

Results & discussion

Chi-NP prefer to internalize into DiI labeled vesicles in primary cortical neurons

To study magnetic forces on intracellular lipid vesicle motion pattern in 48 h cultured primary cortical neurons (E18, rat), chitosan coated superparamagnetic nanoparticles (Chi-NPs) were incubated to enter the neuronal cytosol through cell intrinsic uptake mechanism. We chose chitosan coated functionalized superparamagnetic nanoparticles (Chi-NP) due to their neuroprotective effect.[50, 51] Nanoparticles can enter the neuronal cytosol through active, or passive uptake mechanisms, or diffusive through the cell membrane. Because the surface charge and the hydrodynamic radius highly influences the uptake mechanism,[52] we quantified the surface charge through the zeta-potential and the hydrodynamic radius. The Chi-NP surface charge was cationic in aqueous solution with a hydrodynamic diameter $h_{d,H2O}$ = 210 nm (Zetasizer). In neuronal medium, however, we found that Chi-NPs cluster, most-likely formed a protein corona,[53] which modified their zeta-potential (ζ) from ζ_{H2O} = 11.4±6.0 mV to ζ_{Neuro} = -9.7±0.3 mV and their diameter up to $h_{d,Neuro}$ = 630 nm after 24 h (Fig. 2b), which was also reported in other studies.[54] Thus, primary cortical neurons most-likely respond to cationic nanoparticle clusters.

Based on active, or passive uptake mechanism nanoparticles may end up in early- and late endosomes, lysosomes or other vesicle types (e.g. synaptic vesicles, multi-vesicular endosomes, Fig. 2a2). The association of Chi-NPs with intracellular vesicles in primary cortical neurons was visualized through functionalized green fluorescence (Em: 476 nm, Ex: 490) Chi-NPs co-labeled with four different vesicles markers (late endosome, lysosome, lipophilic dye DiI and DiD labeled intracellular vesicles).

After, six hour incubation with the Chi-NP (30 g/ml), we analyzed 709 fluorescent vesicles in 22 individual neurons from five different neuron preparations. Based on the green signal from the Ch-NPs and the fluorescent signal from labeled vesicles (DiI and DiD), a late-endosomal marker (CellLight Bacmam, Rab7a-RFP) or a lysosomal marker (LysoTracker FarRed), we found Chi-NPs overlapping with 30.0% fluorescent lysosomes, with 44.5 % DiI, with 12.7% DiD labeled vesicles and with 15.5% late endosomes (Fig 2c1, c2, d). When comparing DiI and DiD co-labeled images we observed that most DiI spots do not co-position with DiD spots (Supplementary data, Fig. S4). In contrast, late endosomes overlapped with 90% of the DiD spots (Fig. 2c1) and 43% of the lysosomes overlapped with DiI vesicles. This observation suggests that DiD and DiI labeled intracellular vesicles are not the same type of vesicles. Because we found most Chi-NPs to be located in DiI labeled vesicles, we decided to study the nanomagnetic force effect in neurons in DiI vesicles and to compare our findings to DiD labeled vesicles.

Vesicle trafficking base on the Stokes-Einstein theory depends on the vesicle diameter. Chi-NPs clusters in DiI labeled vesicles and lysosomes presented an average spot diameter of 0.63 μm (range 0.3 – 1.7 μm). NP clusters in the few late-endosome and DiD-labeled vesicles had average spot diameter of 0.7 μm (range of 0.3 – 1.4 μm). Comparing area distribution of DiI and DiD vesicles in neurons incubated with and without Chi-NPs (Supplementary data, Fig. S4b and S4c) did not result in a significant increase of 0.5 μm^2 area sized DiI spots for 0.87 μm NP clusters and even decreased the amount of 0.4 μm^2 area sized DiD spots. Thus, the size of DiI labeled vesicle was not impacted through the uptake or association with Chi-NPs.

In summary, although possessing a large hydrodynamic size, Chi-NPs sequester into the endo-lysosomal network and show highest co-positioning with DiI labeled intracellular vesicles after six hour of incubation without impacting significantly the size of intracellular vesicles in primary cortical neurons.

Magnetic forces preferentially alter lipophilic dye, DiI, stained vesicle motion

Assuming magnetic forces impact vesicle motion locally, we analyzed the position of DiI and DiD labeled vesicle spots in image sequences after six hour nanoparticle exposure before applying and with the magnetic field. While size distribution of uptaken Chi-NP clusters cannot be controlled during experiments, nanomagnetic forces were ensured to remain below 100 pN, by a fixed magnetic element (MEs) design using a previously developed neuromagnetic chip[34] in combination with an externally applied 150 mT (B_{max}) permanent magnet. A poly-l-lysine pattern restricted cell attachment of neurons adjacent to the MEs such that the applied magnetic forces are localized peripheral to the cell nucleus (Fig. 2a3).

Figure 3a shows a representative image sequence of change in position of DiI vesicles carrying Chi-NPs without an intracellular magnetic force stimulus. Co-positioned Chi-NPs move in the same direction as DiI vesicles indicating association or even co-localization, see Supplementary information. The same field of view was then exposed to an external magnetic field (B_{max} = 150 mT, stationary), which immediately altered the vesicle motion pattern due to applied nanomagnetic forces (Fig. 3b, Supplementary data Video V1 and V2). Vesicle displacement was monitored over a 180 s time period at 3 s intervals within a region that included the cell body and neurites (40 μm × 40 μm square), from which vesicle tracking plots were generated using TrackMate[45] (Fig. 3c1 and c2).

From the individual vesicle tracks we analyzed the average vesicle speed (Fig. 3d), space orientation of vesicle tracks (Fig. 3e1 – e3, star plots) and quantified the mean square displacements (MSDs) over a time lag (τ) of 90 s and compared them against MSDs of five potential models: (1) average-sized spherical vesicle, d_h = 300 nm, free diffusive, no viscous restriction; (2) same as (1), with viscous restriction k_{cell} = 0.05, $\eta_{neuron} \approx 0.05\,\eta_{H_2O}$;[55] (3) same as (1), confined restriction; (4) same as (2) for a d_h = 180 nm); and (5) same as (2) for larger intracellular vesicles $d_{h,spot}$ = 800 nm (Fig. 3f1, f2).

Without nanomagnetic forces (no magnetic field, or no fMNPs) the average speed of both DiI and DiD intracellular vesicles was found around 12.5 nm/s and falls in the category of

slow “axonal” (= neurite) transport,[56] in contrast to fast single kinesin motor driven, fast axonal transport of 800 nm/s.[57] With magnetic forces, DiI vesicle speed resulted in averaged 7 nm/s (Fig. 3f, ANOVA for non-normally distributed data $p<0.001$). The reduction of speed can be explained though oppositional acting nanomagnetic forces against the direction of vesicle displacement. The differences in speed reduction between DiI and DiD labeled vesicles can be explained by the difference in association with Chi-NPs. We recall here that 44.5% of all DiI vesicles throughout the neuronal cell body co-positioned with Chi-NPs, but only 12.7% of DiD vesicles (Fig. 2). To test the impact of directed nanomagnetic forces on uni-directional vesicle displacement we compared vesicle motion patterns with and without magnetic field exposure. Figure 3e1 – e3 show the motion pattern in star plots for DiI and DiD vesicles (maximal tracking time of $t_{max} = 114\pm6$ s) loaded with Chi-NPs both with and without an applied magnetic field. We observed that the plot of DiI vesicle tracks altered under the application of a magnetic field. In contrast, DiD vesicle star plots remain very similar (Fig. 3e3).

Furthermore, MSD curves of intracellular DiI vesicles being exposed to Chi-NPs indicate that vesicle motion can be classified as confined diffusive under high viscosity (in cell, Fig. 3f1, f2). Averaging all MSD curves shows a super-diffusive trend for vesicles being exposed to Chi-NPs in contrast to vesicles without nanoparticles (Supplementary data, Figure S5).

In summary, we can conclude that nanomagnetic forces differentially act on DiD and DiI labeled intracellular vesicles in cortical neurons. Specifically, DiI vesicles motility was slowed down significantly due to superimposing nanomagnetic forces blocking the displacement of vesicles uni-directionally.

Nanomagnetic forces outrun biochemical effects on DiI labeled vesicle motion

Lipid vesicles are very important endosomes in neuronal cells when it comes to taking up extracellular components, transporting cargos or exchanging cargos.[48] During these processes vesicles are assumed to be in different motional states, such as totally immobile “docked”, weak diffusive “primed”, or transporting “mobile”, and forces might impact these categories.[11, 13, 22] Therefore, the next question we addressed, is, if we can observe different categories of vesicle motion, and if in our case intracellular forces impact the amount of vesicles in one particular category. To classify and distinguish between “immobile”, “primed” and different “mobile” types of vesicles in our experiments we used a trajectory metric recently introduced by Nofal *et al.* called “caging” diameter[48]. The “caging” diameter (CD) is described as the maximum displacement reached by a vesicle within a specific time frame. Nofal *et al.* used the CD plots versus time plots to identify fluctuation patterns, which they used to discriminate between three types of vesicle motion: “primed” (nearly immobile, or stationary), “caged” (confined diffusion, perpetual motion), and “directed” motion (long-distance)).[58] In our experiment, the time length of 114 s includes fluctuations in speed due to changes between categories, e.g. a mobile vesicle stops and then resumes moving.[22] These fluctuations are best seen when the total traveled length L is also taken into account. Scatter plots of CD versus L demonstrate a larger diversity of molecular movements, which we classified here into five categories: (i) primed, (ii) caged, (iii) primed-transported, (iv) caged-

transported and (v) directed transport based on their trajectory appearance and corresponding threshold values for *CD* and *L* (Fig. 4d).

Under conditions with Chi-NPs but no applied magnetic field (Fig. 4f, N: w/Chi-NP, w/o M), we found 70% of our vesicles motion falling under category I, which corresponds to immobile or docked motion. Furthermore, we found 9% of vesicles in caged motion (category II), 13% in primed-transport motion (category III), 4% with caged and directed motion (category IV) and 5% in directed motion (category V). By applying magnetic forces, ranging from 6 pN to 126 pN (B_{max} = 0.15T, ~ 20 A/m^2, 4 μm × 8 μm ME, h_d = 0.8 μm and 1.5 μm) the number of vesicles shifted within the different motion categories (Fig. 4f). Different motion categories, however, were affected differently. The number of vesicles in direct motion reduced to 0.5%, caged-directed motion reduced to 4.5%, primed-directed motion to 2% and caged motion to 1.3% 67%, which corresponds to a decrease about 90%, 95%, 85% and 67%, respectively. Faster transport categories such as directed and caged-directed were more strongly affected by the magnetic force impact.

Insulin-stimulated vesicles potentiate magnetic force driven orientation of vesicle movement

To further evaluate the link between liposomal vesicle mobility and applied magnetic forces, we altered vesicle motility in two ways: (i) by indirectly activating and (ii) by inhibiting vesicle transport (Fig. 5a). First, we aimed to promote the activation of DiI vesicle dynamics through the addition of 50 nM insulin to the 2 day old cortical neurons in culture (Fig. 5a1). Insulin has been reported to impact the AMPA pathway,[59, 60] and Rab4 pathway. In particular, the former pathway seems to foster internalization of extracellular liquid, or components,[61–63] potentially signaling in cortical neuron to recruit more vesicles for endocytosis and to accelerate the transport of vesicles to ensure increased excocytosis.[42] In Figure 5b1 the star plot, for tracked vesicles upon exposure to insulin and internalized Chi-NP, presents longer trajectories for the same time interval, which indicates an increase in vesicle activity due to faster transport. Looking closer into the different motion categories shows that adding insulin to the neuron culture impacted caged and primed-directed motion most significantly (67%–80%) and increased directed motion about 25% (Fig. 5c1, Experiment: T_1 (no NPs), Chi-Square test = $p<0.05$, h_0: A = N, A: activated, N: no treatment). On top of it, adding Chi-NP significantly increased the amount of directed motion about 270%, Fig. 5c1, T6).

Similar to normal conditions, adding magnetic forces to our activated vesicle motion resulted in 62% more primed vesicle motion (Fig. 5c1, T10). In our opinion, the observed stalling effect is caused by mechanical barriers (the cell membrane) and the imposing of stalling nanomagnetic forces. Assuming an average neurite growth rate of 1 μm/min and perpendicular acting nanomagnetic forces explains well our observation of primed motion within our experimental time frame (114 s). Further indication for the mechanical barrier effect can be found in figure 5b1 (w insulin, w M), where vesicle trajectories show a higher organization of movement directionality following the orientation of the magnetic force vectors. While activation is one way to study interactions between vesicle movement and magnetic forces, another way is to block molecular motors. Using monastrol we aimed to

inhibit vesicle motion based on the assumption of inhibiting anterograde axonal transport mostly involved in neural migration and axonal development.[38–41] Under monastrol exposure (100 μM, B) without the addition of Chi-NP vesicle motion did not change significantly compared to untreated (normal) conditions (Fig. 5c1, T_2 Chi-Square $p > 0.05$, Supplementary data Video V3 – V5). This finding is not surprising as we reported earlier that without nanoparticles MSD was confined diffusive. With the addition of Chi-NPs, however, we observed more vesicles with caged-direct and direct transport motion than without nanoparticles under normal condition (Fig. 5c1, T_6, Chi-Square $p < 0.05$). The treatment with monastrol then significantly altered the proportion of vesicle motion categories (Fig. 5b2, 5 c1, T_8, Chi-Square $p < 0.05$). With the addition of magnetic forces on monastrol treated vesicles the proportion of primed vesicles increased slightly from 86% up to 92%, and resulted in zero directly transported vesicles (Fig. 5b2, 5 c1, T_8, Chi-Square $p < 0.05$). Thus, the applied magnetic forces interfere with vesicle motion independently of intracellular biochemical alterations, but show different effect strengths depending on activated or blocked vesicle motion. Furthermore, our findings are in agreement with biophysical observations *in vitro*, where individual kinesin molecules exhibit 5 - 6 pN stalling force. As we are operating at a force range above 6 pN, it seems that we may modify motor activity enabling us to switch from one motion categories to another and mechanically guiding vesicle transport direction.

To demonstrate control of vesicle transport directionality, we designed a three ME pattern (Fig. 6a1 and a2) such that it produces different force gradients and directions but similar overall forces (Fig. 6a1 versus a2) in comparison to the 6 ME pattern. For both patterns, we found that directed vesicle motion run parallel to the magnetic force axis (Fig. 6c1 and 6 c2). We observed no changes in the proportion of movement categories between the two designs and the proportions of movement categories was independent of the neuron's position relative to the MEs (Fig. 6d1, d2, e: T_5, e: T_6, Chi-square, $p>0.05$). Therefore, these findings indicate that with a given force magnitude, the number of motion categories remain the same, however, the orientation of vesicle motion can be engineered by modulating the magnetic force vector direction.

Surface functionalization of nanoparticles impacts intracellular vesicle motion pattern

Nanoparticles are entering mammalian cells through a cellular membrane using a diverse range of uptake mechanisms such as phagocytosis, micropinocytosis, clathrin- or caveolae-mediated endocytosis, or direct penetration.[53, 64, 65] Anionic nanoparticle clusters have been reported to utilize caveolae-mediated endocytosis with a high proportion getting sorted into lysosomes in epithelial cells.[52] Further, the amount of surface charge seems to have an impact on the uptake mechanism in neuroblastoma cells and intracellular particle location.[66] To test the impact of magnetic forces on vesicle motion induced by nanoparticles with different surface charges, we incubated the 2 day old cortical neurons with starch-coated, fluorescently-labeled, superparamagnetic nanoparticles (D-NP, $\zeta_{Neuro} = -0.03 \pm 0.3$ mV) for six hour. It was reported previously that starch-coated nanoparticles are less likely to pass the neuronal cell membrane.[67, 68] Thus, we assumed that DiI vesicle motion remains unaffected when exposed to starch-coated nanoparticles. The difference in vesicle motions between Chi-NPs and D-NPs are shown in star plots in Figure 7. Without a magnetic field

DiI vesicles show similar movement patterns independent on the surface charge of the nanoparticles. Only the effect of increase in velocity of DiI vesicles (Fig. 3) when exposed to Chi-NPs was not observable for D-NPs. With magnetic field, the weaker anionic D-NPs have the same potential to generate magnetic forces, however, we observed only 24% reduction in vesicle motion, which can also be explained by a slight alteration in vesicle motion categories induced by the magnetic field in the absence of fMNPs (Fig. 5 c1, T_3, Chi-Square: $p < 0.05$ h_0: no M = w M).

In control studies (no Chi-NPs) performed in primary rat cortical neurons we observed a small but significant increase in primed and caged vesicles solely attributed to the application of the magnetic field (Fig. 6 c1, c2, e: $T_{3,4}$, e: $T_{8,9}$, Chi-square, $p < 0.05$). A possible explanation can come from the “tug of war” model, which proposes a diffusive state, when none of the molecular motors are bound to microtubules.[26] Forces much below the pico-newton range could in such a diffusive state locally trap or guide vesicle motion.[69] During an unbound state, a magnetic Lorentzian force, due to the charged nature of the vesicle, may induce circular vesicle motion, which we observe as trapped vesicle motion. Alternatively, it has been suggested that cortical neurons of rodents might carry iron oxide content derived from dissociation reactions of iron content,[70, 71] which can potentially interact with a bulk magnetic field. To test if cortical neurons from other species exhibit similar behavior we cultured human neuronal cells derived from human induced pluripotent stem cells (hiPS) on our neuromagnetic platform and compared their vesicle motion after 2 days *in vitro* to the one in rat cortical neurons under magnetic gradient exposure (no nanoparticles, see supplementary data for figure S2, Video V6 and V7). Without fMNPs human neurons showed a significant difference in vesicles motion, specifically for directed transport (Cat V, Supplementary data: Fig. S2) compared to rat neurons. Furthermore, the application of a magnetic field on human neurons resulted in no significant changes of overall vesicle motion behavior.

Conclusions

In conclusion, we have designed a method to alter the motion of lipophilic dye labeled vesicles in rat embryonic cortical neurons by applying magnetic forces on cell-internalized chitosan coated superparamagnetic nanoparticles. We provide evidence that our chitosan coated nanomagnets preferentially associate with DiI labeled intracellular vesicles after six hour of incubation and impact their motion pattern. Using our novel micromagnetic chip, we align cortical neurons to embedded MEs using protein patterns, and study the effects of localized nanomagnetic forces ranging from 6 to 120 pN on lipid vesicle dynamics in primary rat cortical neurons. We observed vesicle transport by tracking vesicle trajectories and utilized a caging diameter metric in combination with total traveled length to quantify transport activity. Applying these new metrics to our experimental data, we were able to define five distinguishable categories of vesicle movement, which can be compared to previously reported classifications: primed, docked, primed-directed, docked-directed and directed movement patterns. Super-imposing the nanomagnetic-mediated physical stalling force or re-directing force on vesicles outrun the biochemically stimulation effect through chemical activation and inhibition of vesicle movement. Beyond this point, we observed that the type of surface charge at the shell of the nanomagnets has an impact on the location of

where the nanomagnetic forces act and therefore impacted the force effect on vesicle motion patterns. Controversially, in rat cortical neurons vesicle motion seems to be sensitive to bulk magnetic fields (150 mT), without the presence of nanomagnets, but not in human excitatory neurons. Having shown a link between applied magnetic forces and vesicle dynamics, now opens the possibility to connect magnetic forces to protein formation, cytoskeletal changes and intracellular signaling pathways in neurons in the future. As a consequence, future study can be targeted to spatially and temporally control transport and signaling events in cortical neurons such as inhibiting the propagation of tangles of the microtubules-associated protein Tau, or re-orienting cytoskeleton structure after injury. In a broader perspective, controlling vesicle motion locally and intracellularly by magnetic forces can bring many benefits to pharmacological treatments, where temporal and spatial cell signal administering are crucial.

Supplementary Material

Refer to Web version on PubMed Central for supplementary material.

Acknowledgments

The authors wish to thank the California NanoSystems Institute and the UCLA Flow Cytometry Core Laboratory for providing access to the Center for Micro- and Nanofabrication and the Flow Cytometer, respectively. We thank Dr. D. Zosso for debugging and optimizing MATLAB code for trajectory analysis. Dr. P. Tseng is acknowledged for technical advice on-chip fabrication and J. Harrison for electroplating maintenance. We thank Dr. Wu for providing access to the Zetaziser. The authors thank Dr. MD. R. Kulkarni for scientific discussion and Dr. E. Diebold for providing access to high resolution objectives for microscopic imaging. A.K. thanks the Swiss National Science Foundation (SNSF) for supporting this project under the grant P300P2_147753. Further, this work was partially supported through the NIH Director's New Innovator grant (1DP2OD007113) for D.D.

References

1. Tyler WJ. Nat Rev Neurosci. 2012; 13:867–878. [PubMed: 23165263]
2. Loewenstein WR. Annals of the New York Academy of Sciences. 1959; 81:367–387. [PubMed: 14417922]
3. Hilgetag CC, Barbas H. Plos Computational Biology. 2006; 2:146–159.
4. Holland M, Miller K, Kuhl E. Ann Biomed Eng. 2015:1–14. [PubMed: 25527321]
5. Polleux F, Snider W. Cold Spring Harbor Perspectives in Biology. 2010:2.
6. Pfister BJ, Iwata A, Meaney DF, Smith DH. The Journal of Neuroscience. 2004; 24:7978–7983. [PubMed: 15356212]
7. Kilinc D, Blasiak A, O'Mahony JJ, Lee GU. Sci Rep. 2014:4.
8. Nguyen TD, Hogue IB, Cung K, Purohit PK, McAlpine MC. Lab on a Chip. 2013; 13:3735–3740. [PubMed: 23884453]
9. Lamoureux P, Ruthel G, Buxbaum RE, Heidemann SR. The Journal of Cell Biology. 2002; 159:499–508. [PubMed: 12417580]
10. Heidemann SR, Bray D. Frontiers in Cellular Neuroscience. 2015:9. [PubMed: 25698924]
11. Ahmed WW, Saif TA. Sci Rep. 2014:4.
12. Franze K. Development. 2013; 140:3069–3077. [PubMed: 23861056]
13. Ahmed WW, Li TC, Rubakhin SS, Chiba A, Sweedler JV, Saif TA. Cellular and molecular bioengineering. 2012; 5:155–164. [PubMed: 23002399]
14. Jerel KM, William JT. Physical Biology. 2014; 11:051001. [PubMed: 25156965]
15. Ingber DE. The FASEB Journal. 2006; 20:811–827. [PubMed: 16675838]
16. Bray D. Developmental Biology. 1984; 102:379–389. [PubMed: 6706005]
17. Lamoureux P, Heidemann S, Miller KE. J Vis Exp. 2011; :e2509.doi: 10.3791/2509

18. Kilinc D, Lee GU. Integrative Biology. 2014; 6:27–34. [PubMed: 24263142]
19. Pine J, Chow G. Biomedical Engineering, IEEE Transactions on. 2009; 56:1184–1188.
20. Lipfert J, Hao X, Dekker NH. Biophysical Journal. 2009; 96:5040–5049. [PubMed: 19527664]
21. Fass JN, Odde DJ. Biophysical journal. 2003; 85:623–636. [PubMed: 12829516]
22. Ahmed WW, Williams BJ, Silver AM, Saif TA. Lab on a Chip. 2013; 13:570–578. [PubMed: 23303380]
23. Tay A, Kunze A, Jun D, Hoek E, Di Carlo D. Small. 2016; 12:3559–3567. [PubMed: 27228954]
24. Vance JE, Campenot RB, Vance DE. Biochimica et Biophysica Acta (BBA) - Molecular and Cell Biology of Lipids. 2000; 1486:84–96. [PubMed: 10856715]
25. Hirokawa N, Niwa S, Tanaka Y. Neuron. 2010; 68:610–638. [PubMed: 21092854]
26. Hancock WO. Nat Rev Mol Cell Biol. 2014; 15:615–628. [PubMed: 25118718]
27. Stiess M, Bradke F. Developmental Neurobiology. 2011; 71:430–444. [PubMed: 21557499]
28. Bradke F, Dotti CG. Neuron. 1997; 19:1175–1186. [PubMed: 9427242]
29. Zempel H, Mandelkow E. Trends in Neurosciences. 2014; 37:721–732. [PubMed: 25223701]
30. Dixit R, Ross JL, Goldman YE, Holzbaur ELF. Science. 2008; 319:1086–1089. [PubMed: 18202255]
31. Stamer K, Vogel R, Thies E, Mandelkow E, Mandelkow EM. The Journal of Cell Biology. 2002; 156:1051–1063. [PubMed: 11901170]
32. Ebneth A, Godemann R, Stamer K, Illenberger S, Trinczek B, Mandelkow EM, Mandelkow E. The Journal of Cell Biology. 1998; 143:777–794. [PubMed: 9813097]
33. Trinczek B, Ebneth A, Mandelkow EM, Mandelkow E. Journal of Cell Science. 1999; 112:2355–2367. [PubMed: 10381391]
34. Kunze A, Tseng P, Godzich C, Murray C, Caputo A, Schweizer FE, Di Carlo D. ACS Nano. 2015; 9:3664–3676. [PubMed: 25801533]
35. Tseng P, Judy JW, Di Carlo D. Nat Meth. 2012; 9:1113–1119.
36. Pinkernelle J, Calatayud P, Goya G, Fansa H, Keilhoff G. BMC Neuroscience. 2012; 13:32. [PubMed: 22439862]
37. Pisanic TR II, Blackwell JD, Shubayev VI, Fiñones RR, Jin S. Biomaterials. 2007; 28:2572–2581. [PubMed: 17320946]
38. Lin S, Liu M, Son Y-J, Timothy Himes B, Snow DM, Yu W, Baas PW. Traffic. 2011; 12:269–286. [PubMed: 21166743]
39. Lakämper S, Thiede C, Düselder A, Reiter S, Korneev MJ, Kapitein LC, Peterman EJG, Schmidt CF. Journal of Molecular Biology. 2010; 399:1–8. [PubMed: 20227420]
40. Gartner M, Sunder-Plassmann N, Seiler J, Utz M, Vernos I, Surrey T, Giannis A. ChemBioChem. 2005; 6:1173–1177. [PubMed: 15912555]
41. Haque SA, Hasaka TP, Brooks AD, Lobanov PV, Baas PW. Cell Motility and the Cytoskeleton. 2004; 58:10–16. [PubMed: 14983520]
42. Imamura T, Huang J, Usui I, Satoh H, Bever J, Olefsky JM. Molecular and Cellular Biology. 2003; 23:4892–4900. [PubMed: 12832475]
43. Rhee YH, Choi M, Lee HS, Park CH, Kim SM, Yi SH, Oh SM, Cha HJ, Chang MY, Lee SH. Cell Death Dis. 2013; 4:e766. [PubMed: 23928705]
44. Thevenaz P, Ruttimann UE, Unser M. Image Processing, IEEE Transactions on. 1998; 7:27–41.
45. Perry, N., Tinevez, J-Y., Schindelin, J. [accessed 6/4/2015] TrackMate - Fiji. http://fiji.sc/TrackMate
46. Chenouard N, Smal I, de Chaumont F, Maska M, Sbalzarini IF, Gong Y, Cardinale J, Carthel C, Coraluppi S, Winter M, Cohen AR, Godinez WJ, Rohr K, Kalaidzidis Y, Liang L, Duncan J, Shen H, Xu Y, Magnusson KEG, Jalden J, Blau HM, Paul-Gilloteaux P, Roudot P, Kervrann C, Waharte F, Tinevez JY, Shorte SL, Willemse J, Celler K, van Wezel GP, Dan HW, Tsai YS, de Solorzano CO, Olivo-Marin JC, Meijering E. Nat Meth. 2014; 11:281–289.
47. Monnier N, Guo SM, Mori M, He J, Lénárt P, Bathe M. Biophysical Journal. 2012; 103:616–626. [PubMed: 22947879]

48. Nofal S, Becherer U, Hof D, Matti U, Rettig J. The Journal of Neuroscience. 2007; 27:1386–1395. [PubMed: 17287513]
49. Preacher KJ. Journal. 2001
50. Pangestuti R, Kim SK. Marine Drugs. 2010; 8:2117–2128. [PubMed: 20714426]
51. Cho Y, Shi R, Ben Borgens R. Journal of Biological Engineering. 2010; 4:2. [PubMed: 20205817]
52. Harush-Frenkel O, Rozentur E, Benita S, Altschuler Y. Biomacromolecules. 2008; 9:435–443. [PubMed: 18189360]
53. Lynch I, Salvati A, Dawson KA. Nat Nano. 2009; 4:546–547.
54. Tay A, Kunze A, Jun D, Hoek E, Carlo DD. Small. 2016
55. Popov S, Poo M. The Journal of Neuroscience. 1992; 12:77–85. [PubMed: 1370324]
56. Konzack S, Thies E, Marx A, Mandelkow EM, Mandelkow E. The Journal of Neuroscience. 2007; 27:9916–9927. [PubMed: 17855606]
57. Svoboda K, Block SM. Cell. 1994; 77:773–784. [PubMed: 8205624]
58. Ott D, Bendix PM, Oddershede LB. ACS Nano. 2013; 7:8333–8339. [PubMed: 24116711]
59. Song I, Huganir RL. Trends in Neurosciences. 2002; 25:578–588. [PubMed: 12392933]
60. Arevalo MA, Rodríguez-Tébar A. Molecular Biology of the Cell. 2006; 17:3369–3377. [PubMed: 16723502]
61. Hoerndli, Frédéric J., Wang, R., Jerry, E., Kallarackal, A., Brockie, Penelope J., Thacker, C., Madsen, David M., Maricq, Andres V. Neuron. 2015; 86:457–474. [PubMed: 25843407]
62. Hoerndli, Frédéric J., Maxfield, Dane A., Brockie, Penelope J., Mellem, Jerry E., Jensen, E., Wang, R., Madsen, David M., Maricq, Andres V. Neuron. 2013; 80:1421–1437. [PubMed: 24360545]
63. Chen TJ, Wang DC, Hung HS, Ho HF. Cell Mol Life Sci. 2014; 71:4069–4080. [PubMed: 24705985]
64. Chou LYT, Ming K, Chan WCW. Chemical Society Reviews. 2011; 40:233–245. [PubMed: 20886124]
65. Dawson KA, Salvati A, Lynch I. Nat Nano. 2009; 4:84–85.
66. Calatayud MP, Sanz B, Raffa V, Riggio C, Ibarra MR, Goya GF. Biomaterials. 2014; 35:6389–6399. [PubMed: 24816288]
67. Tay A, Kunze A, Jun D, Hoek E, Di Carlo D. Small. 2016; n/a-n/a. doi: 10.1002/smll.201600673
68. Tay A, Kunze A, Murray C, Di Carlo D. ACS Nano. 2016; 10:2331–2341. [PubMed: 26805612]
69. Etoc F, Vicario C, Lisse D, Siaugue JM, Piehler J, Coppey M, Dahan M. Nano Letters. 2015; 15:3487–3494. [PubMed: 25895433]
70. Hill JM, Ruff MR, Weber RJ, Pert CB. Proceedings of the National Academy of Sciences of the United States of America. 1985; 82:4553–4557. [PubMed: 2989832]
71. Hill JM, Switzer RC III. Neuroscience. 1984; 11:595–603. [PubMed: 6717804]

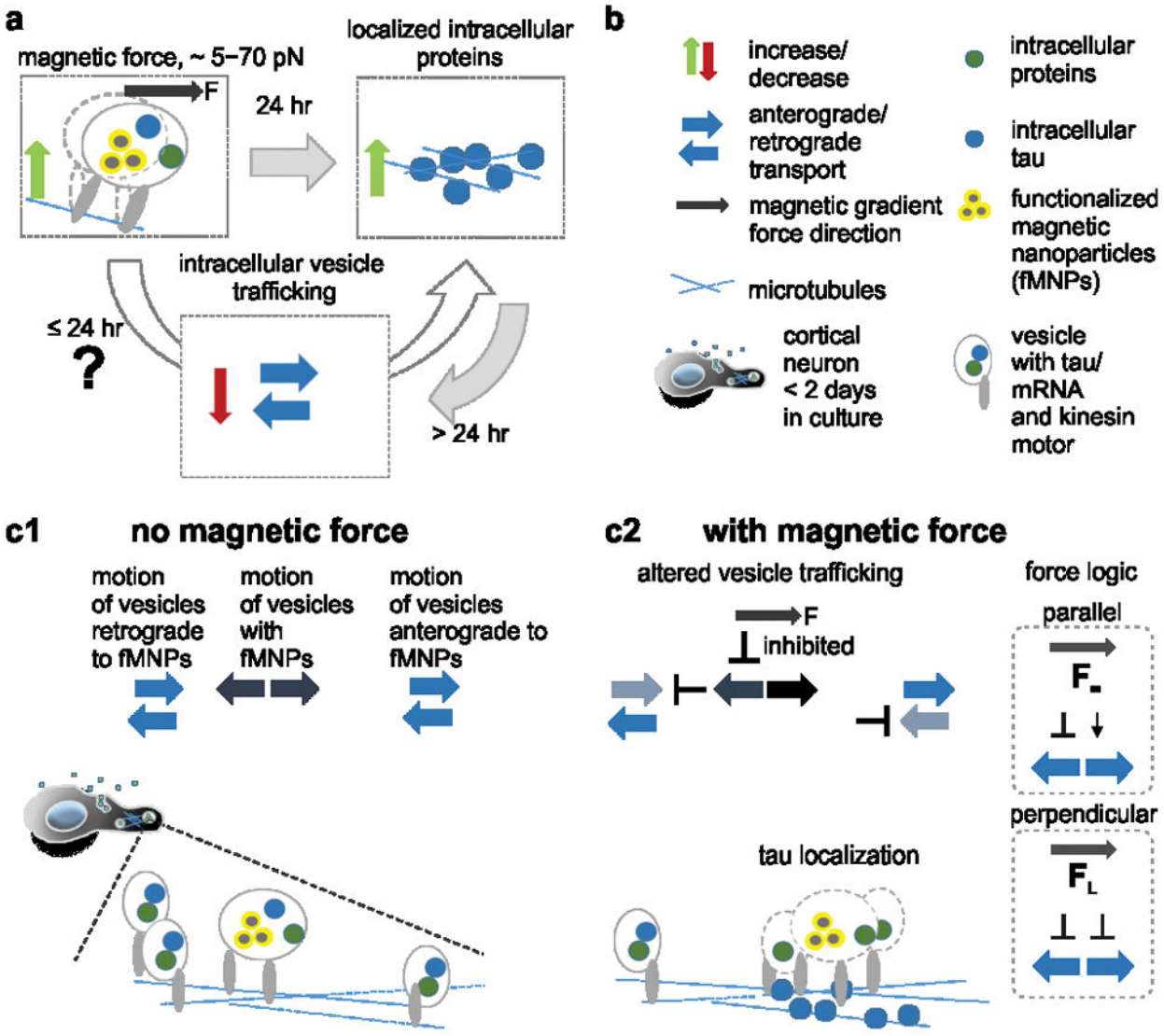

Figure 1.

Controlling vesicle trafficking through magnetic forces. (a) Magnetic forces can establish intracellular protein gradients in cortical neurons, probably due to an altered intracellular trafficking mechanism. While cellular response to a chronic stimulus might be delayed, we want to study here the impact of magnetic forces below 24 h within cortical neurons immediately after applying the magnetic force stimulus. (b) Legend for schematic. (c1 – c2) Schematic demonstrates the altered trafficking hypothesis, where fMNPs get transported within vesicles along microtubules using based on directed (molecular motor driven), or diffusive processes and interfere with superimposed stalling forces under the application of a permanent magnetic fields. (c1) Without magnetic forces vesicle motion follow anterograde and retrograde routes. (c2) With magnetic field gradients local vesicle trafficking can get blocked (perpendicular), or de-/accelerated in a specific direction (parallel) due to the mechanical interplay of vesicles filled with fMNPs.

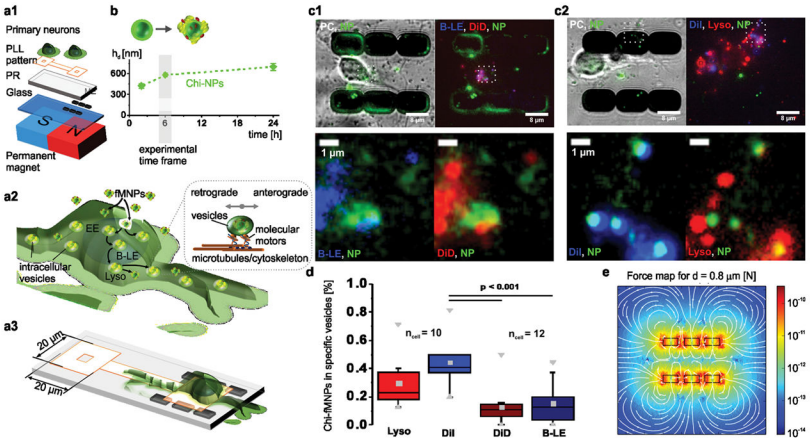

Figure 2.

Chitosan-functionalized magnetic nanoparticles (fMNPs) heap up in DiI labeled intracellular vesicles. (a1) A chip-based approach facilitates a highly parallelized single cellular study of vesicle interactions with fMNPs and magnetic forces. The chip has quadratic poly-l-lysine patterns (PLL) aligned on top of magnetic elements (MEs) or several micrometers spaced apart. (a2) Schematic shows potential routes for intracellular uptake of fMNPs and their location in different vesicle types dependent on their uptake mechanism. EE = early endosomes, B-LE = late endosomes, Lyso = lysosomes, Vesicles = lipid, membrane, synaptic, receptor vesicles. (a3) Single cell and magnetic element pattern assembly. (b) Changing hydrodynamic diameter over time of Chi-fMNP (green) and D-fMNP (red) clusters in neurobasal media (+B-27, +GlutaMAX). (c1 & c2) False-colored fluorescent images show co-labeling of different vesicles with Chi-fMNPs in primary cortical neurons (E18, 2 DIV) on-chip. Chi-fMNPs are green fluorescent. DiD (red) and DiI (blue) stained unspecified different types of lipid vesicles. B-LE (blue) stained late endosomes and Lyso (red) lysosomes. (d) Relative count of Chi-fMNPs located in specific vesicle types. NNP = 86 (Lyso/DiI images), NNP = 55 (DiD/BLE). (e) COMSOL/MATLAB based computed magnetic force field 1 µm above two 3-rowed magnetic element pattern (Bmax = 150 mT, nanoparticle cluster diameter d = 0.8 µm).

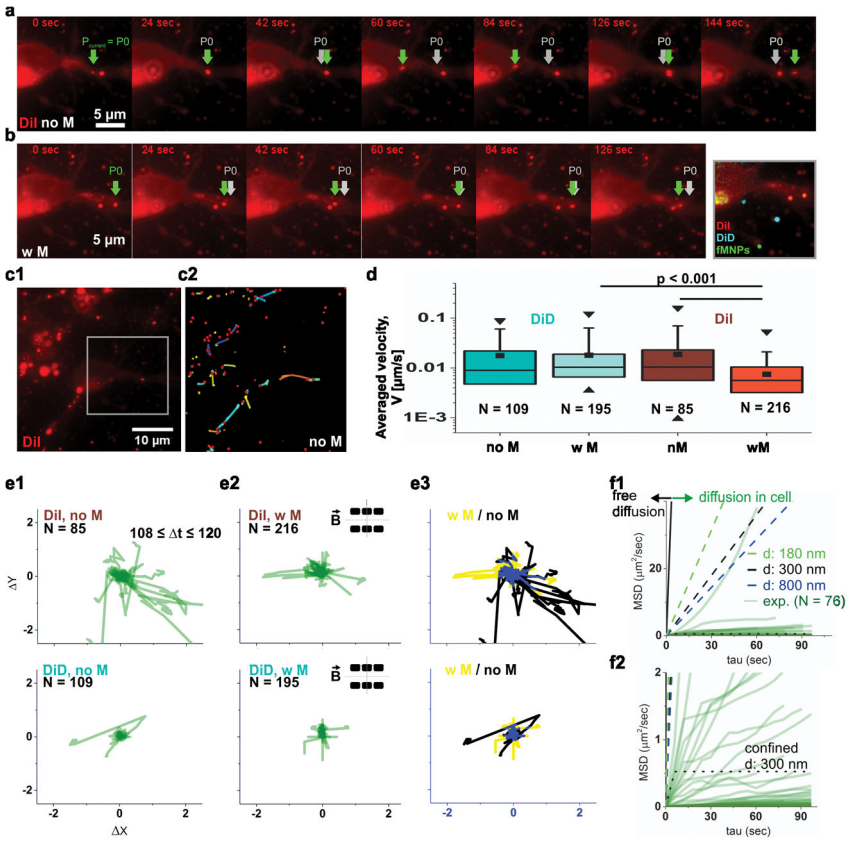

Figure 3.

DiI-stained lipid vesicles respond to Chi-fMNP induced magnetic forces. (a) Image sequence of DiI labeled cortical neuron (E18, 2 DIV) highlights an active moving vesicle without superimposed magnetic forces (no M). P0: start position = arrow at t = 0 sec. Green arrow indicates time specific current position. (b) Image sequence of the same neuron applied to magnetic fields (w M) inducing magnetic forces on Chi-fMNP-loaded vesicles (yellow/orange due to red - DiI and green -fMNP co-localization). (c1) Image region of interest above 6 pattern MEs used for tracking vesicle motion. (c2) Vesicle track map of automatic detected vesicles and generated tracks. (d) Averaged velocities (box-lot) of DiI and DiD-labeled vesicles were monitored with and without superimposed magnetic forces. (e1 – e3) Centered vesicle trajectories of tracked DiD and DiI vesicles were extracted from the same cortical neuron (e1) with (w M), (e2) without magnetic forces (no M), and in (e3) shown as XOR plots. (f1, f2) Mean-square displacement diagram (MSD) shows MSD values for individual tracks (exp. data) in comparison with free diffusion (outside the cell), diffusion within the cytoplasm (diffusion in cell), and confined diffusion within the cytoplasm (confined).

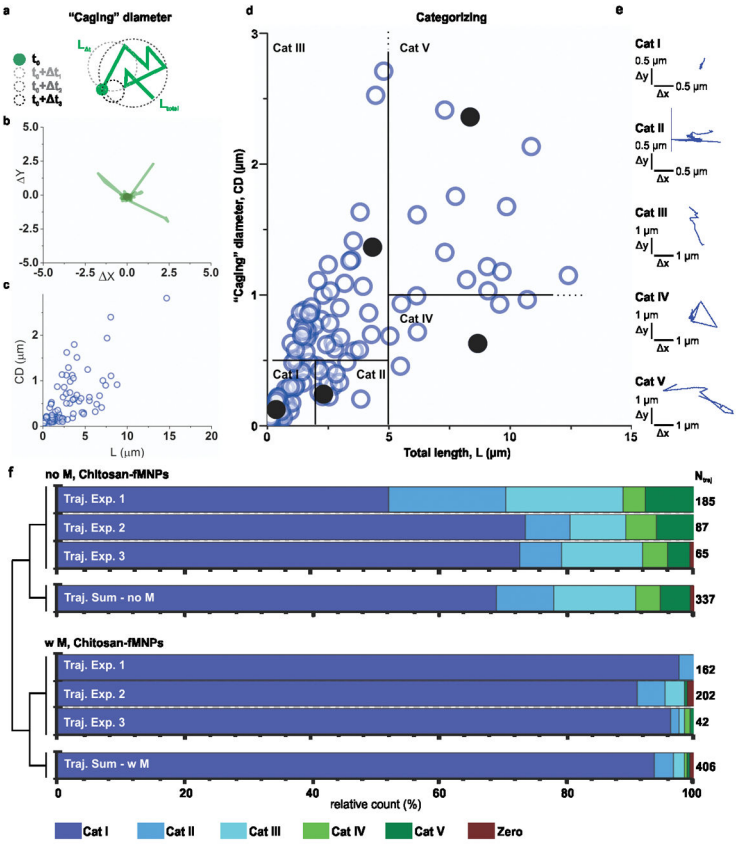

Figure 4.

Classifying vesicle motion based on a “caging diameter” exhibits a more diverse range of motion patterns in contrast to the MSD. (a) Vesicle example and definition of caging diameter. (b) One set of centered DiI vesicle tracks. (c) Scatter plot of averaged “caging” diameter (CD) over total traveled length (L) within sec. (d) CD-L plot used to categorize vesicle tracks based on five characteristic trajectory paths separated by numerical thresholds (horizontal and vertical lines). (e) Five different vesicle track categories corresponding to the black dots in (d): Cat I: docked, Cat II: caged, Cat III: mixed transport, Cat IV: caged with directed motion, Cat V: directed transport. (f) Bar histogram plot of relative counts per category for three independent experiments. Zero: no motion/totally immobilized. Ntraj = total number of trajectories per ROI, w M with magnetic field, no M no magnetic field.

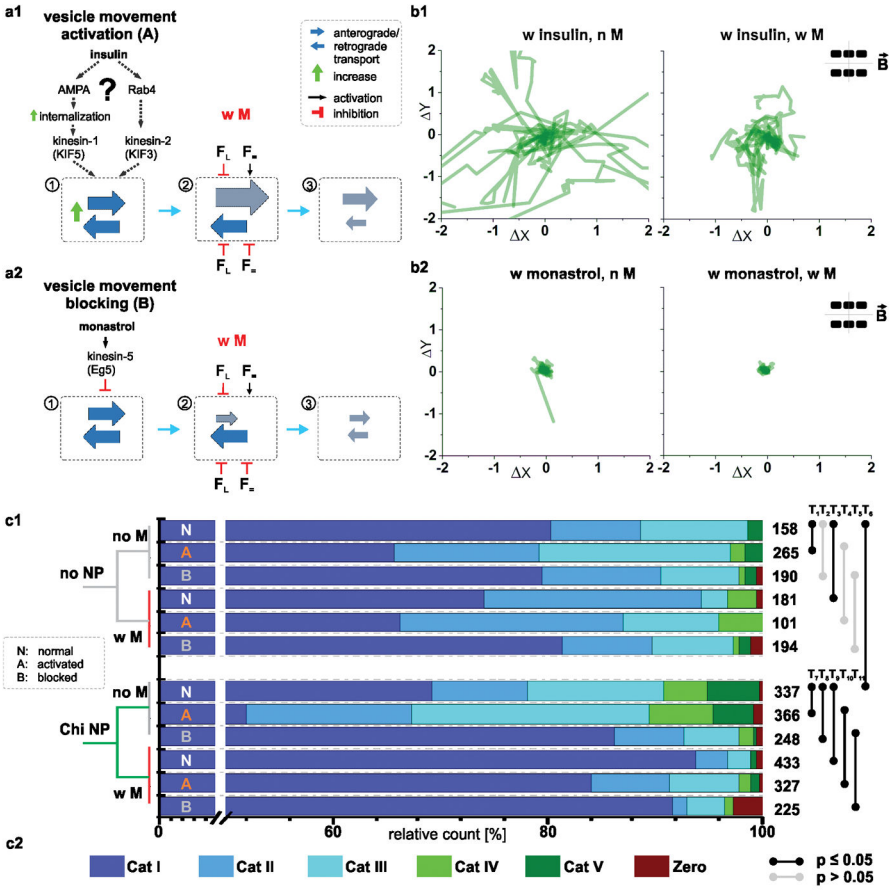

Figure 5.

Magnetic forces superimpose chemical signaling induced changes in DiI vesicle motion. (a) Vesicle motion can be accelerated or blocked using (a1) insulin or (a2) monastrol. (b1) Centered vesicle track plot shows insulin effect on DiI vesicle motion. (b2) Centered vesicle track plot shows monastrol effect on DiI vesicle motion. (c1) Bar histogram plot (H) of relative counts per category for DiI vesicle tracks containing no fMNPs (no NP), containing fMNPs (Chi NP) without a chemical treatment (N), under addition of insulin (A), treated with monastrol (B) without magnetic forces (no M) with superimposed magnetic field (w M). Total number of trajectories are shown right to the bar plot. Line-connectors demonstrate statistical test result (p-value) for Chi-Square test with e.g. h0: HnoNP = HChi NP for T6. (c2) Category legend: Cat I: docked, Cat II: caged, Cat III: docked-transport, Cat IV: caged with directed motion, Cat V: directed transport, Zero: no motion/totally immobilized.

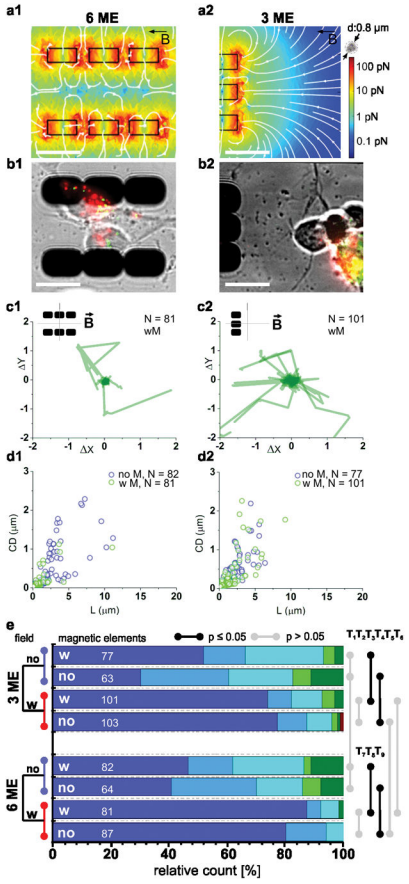

Figure 6.

Magnetic field gradient direction primarily impacts force direction but not DiI vesicle motion pattern categories. (a1) COMSOL simulation of force gradient with six and (a2) with three magnetic element (ME) patterns. (b1) Representative phase contrast image overlaid with fluorescent shows cortical neurons cultured on top of the six and (b2) three ME pattern with DiI (red) vesicles containing partially fMNPs (green). Scale bar = 10 µm. (c1) Centered vesicle tracks with magnetic force impact above two three-rowed ME pattern and (c2) one three-rowed ME pattern. (d1) CD-L plot for tracked vesicles above six and (d2) three MEs with (w M) and without magnetic force (no M). (e) Bar histogram plot (H) of relative counts per category for DiI vesicle tracks above (w ME) and 100 µm spaced apart (no ME) from three (3 ME) and six (6 ME) magnetic element patterns with (w) and without (no) magnetic field. Total number of trajectories are shown right to the bar plot. Line-connectors demonstrate statistical test result (p-value) for Chi-Square test with h0: H3ME = H6ME.

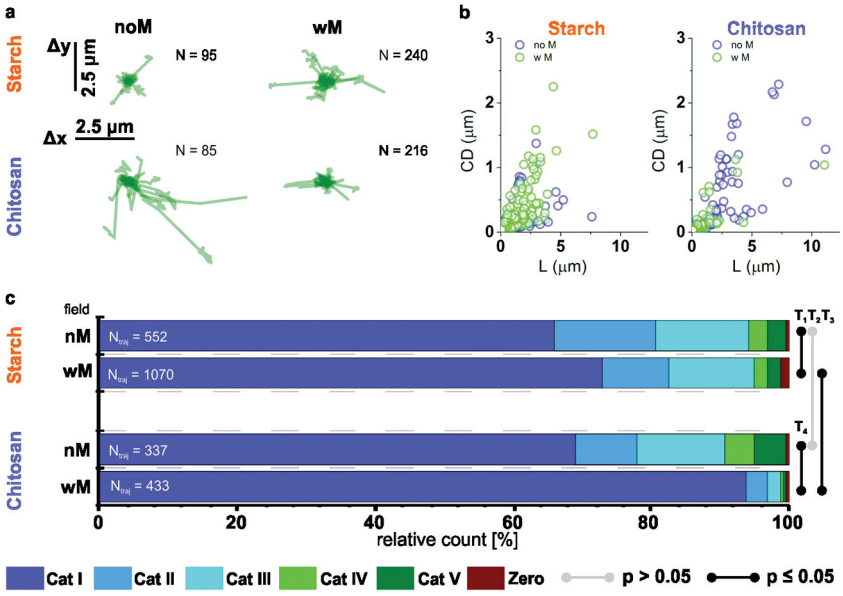

Figure 7.

Nanoparticle surface charge impacts the magnetic force effect on DiI labeled vesicle motion. (a) Center plot of DiI labeled vesicle tracks after exposure to chitosan or starch coated fMNPs without (no M) and with (w M) superimposed magnetic forces. (b) Caging diameter over length diagram for DiI labeled vesicles after starch or chitosan fMNPs exposure with (w M) and without (no M) magnetic impact. (c) Bar histogram plot (H) of relative counts per category for DiI vesicle tracks with chitosan or starch fMNPs above six ME pattern with (w M) and without (n M) magnetic field. Ntraj = total number of trajectories. Line-connectors demonstrate statistical test result (p-value) for Chi-Square test with h0: Hchitosan = Hstarch.